RESEARCH ARTICLE

SPE INSPIRING PLASTICS PROFESSIONALS | POLYMER ENGINEERING AND SCIENCE | WILEY

Novel, solvent-based method for the production of polymer sheets with a superhydrophobic surface

Csenge Vámos[1,2] | Ilona Rácz[2] | Tamás Bárány[1] | Alfréd Menyhárd[3] | Botond Béla Marosfői[2]

[1]Department of Polymer Engineering, Faculty of Mechanical Engineering, Budapest University of Technology and Economics, Budapest, Hungary

[2]Furukawa Electric Institute of Technology Ltd, Budapest, Hungary

[3]Department of Physical Chemistry and Materials Science, Faculty of Chemical Technology and Biotechnology, Budapest University of Technology and Economics, Budapest, Hungary

Correspondence
Csenge Vámos, Department of Polymer Engineering, Faculty of Mechanical Engineering, Budapest University of Technology and Economics, Műegyetem rkp. 3, Budapest H-1111, Hungary.
Email: csenge.vamos@furukawaelectric.com

Abstract

We have introduced a novel solvent-based method to roughen polymer surfaces and characterized treated polypropylene (PP). The method consists of three main steps: solvent treatment, drying, and peeling. We investigated the effects of process parameters such as time of immersion in the solvent, solvent temperature, and drying temperature on the surface morphology created. The structure formed on the surface is mainly influenced by solvent temperature and drying temperature. We also characterized the wetting behavior of the surfaces. The patterned surfaces exhibit superhydrophobic characteristics with a high water contact angle (CA) (>155 °) and low water contact hysteresis (<5°). Adding an effective nucleating agent to PP makes it possible to generate outstanding CAs (>160°) and tailor spherulite sizes. The method is simple and scalable, therefore this superhydrophobic material is easy to mass-produce.

KEYWORDS

crystallization, hierarchically structured surface, peeling, polypropylene, skin layer, superhydrophobicity

1 | INTRODUCTION

Superhydrophobic (with water contact angle (CA) exceeding 150°) and water-repellent surfaces (hysteresis below 10°) are fascinating and widely used,[1] their uses ranging from self-cleaning surfaces[2] and anti-ice coatings[3] to anti-corrosion surfaces[4,5] and membranes.[6,7] The formation of superhydrophobic surfaces is essentially determined by two crucial parameters, appropriate surface roughness and low surface energy.[8,9]

Surface roughness alters the CA measured on a heterogeneous surface according to two typical models: the Wenzel[10] and Cassie-Baxter[11] theories.

So far, various techniques[12–18] have been applied to produce superhydrophobic surfaces on polymers by creating well-ordered structures. Of these solvent-based techniques,[19–24] such as phase separation methods[25–28] belong to a unique group. In the phase separation method, a roughened surface is prepared with micro-and nanoscale roughness; the properties of a homogeneous solution are

changed, such as temperature, components, and concentration. When the solvent is removed from the system, the remaining solid phase forms the patterned structure.[29,30] Phase separation methods can be classified according to the ways of initiating the phase separation process. In the case of thermally-induced phase separation (TIPS), phase separation or crystallization occurs when the temperature of the solvent is reduced.[31] A large number of publications investigate the effects of the processing parameters of TIPS on surface structure formation. These processing parameters include solution concentration and temperature,[32] the molecular weight of polymer,[33] and cooling conditions.[34] Many different textures can be produced by altering the concentration of the polymer solution. Typically, a dilute polymer solution produces a surface with cellular morphology, while a highly concentrated solution or gels lead to sphere-like structures.[30] The main advantages of phase separation methods are that they are easy to reproduce and control, and the structure is less prone to defects. TIPS can be best used with semi-crystalline polymers.[35–37] Since it is simple, it is also cost-effective in industrial-scale production.[38,39]

Polypropylene (PP) is one of the most widely used semi-crystalline polymers. Due to its good mechanical properties, excellent solvent resistance, low cost, and inherent hydrophobic nature, PP is an extensively studied conventional polymer.[40] These properties make PP a great candidate for use with our technology.

Extruded PP products are widely used in electronics, food packaging, construction, and many other areas.[41] A roughened surface on these extruded products imbues them with new properties, which opens up new application areas.

Methods for producing roughened structured surfaces on PP using TIPS are becoming more widespread.[32,42,43] Many studies give a comprehensive overview of how crystallization depends on the tacticity and molecular weight of PP,[44–46] and how the structure and properties can be adjusted by changing the treatment conditions, such as solvent type and its temperature,[47] solution concentration[31,48] and cooling temperature.[49,50]

Several phase separation–based technologies are used to form the superhydrophobic coating on the surface of a selected substrate.[51,52] In these cases, an additional step may be required to increase interfacial adhesion between the substrate and the deposited layer to prevent exfoliation, which would further complicate the technology.[53] Moreover, the adhesion between the substrate and the roughened coating also has to be considered for better usability. Creating the rough surface directly from the substrate would simplify the method and eliminates adhesion problem between the substrate and roughened layer.

This study introduces an easy-to-perform, low-cost technology for preparing hierarchically structured surfaces on extruded PP sheets via a method involving solvent treatment, drying, and peeling.

With the method presented,[54] an integrated outer layer forms on the surface of the sample similar to the skin layer of asymmetric membranes,[55–57] which are often produced with the TIPS method. Asymmetric membranes represent a specific group of membranes where a thin skin layer forms on the porous layer.[58–60] Tuning of the formation of the skin layer or eliminating it is highly favorable for the optimization of the membrane permeability and surface wettability.[61,62] With this novel technology, we can remove this skin layer easily to exploit the superhydrophobicity of the underlying surface.

This paper describes the structure and the correlations between processing parameters and the morphology created, such as the effect of solvent temperature and immersion time on spherulite size, the thickness of the skin and porous layer, and the effect of the drying temperature on spherulite size and the removability of the skin layer. We also investigated the effect of a nucleating agent for PP on the morphology of the surface. The morphology was investigated by scanning electron microscopy and polarized optical microscopy. The wettability of the created surfaces was characterized with a CA goniometer. To the best of our knowledge, this unique method on PP sheets has not been previously investigated. We strongly believe that this method can effectively form tunable structured surfaces in mass production as well.

2 | EXPERIMENTAL

2.1 | Materials

PP homopolymer (Tipplen H681F, MOL Petrochemicals Co. Ltd., Hungary) with a melt flow rate (MFR) of 1.7 g/10 min. A non-soluble nucleating agent was ADK STAB NA-21 E (Adeka, Tokyo, Japan). The nucleating agent was added to the polymer in amounts of 50 to 1000 ppm. Xylene (mixture of isomers, purity 98%) was supplied by VWR Chemicals, Germany, and used as received.

2.2 | Experiments

We extruded 1 mm PP sheets with a co-rotating twin-screw extruder (TSA, Cernobbio, Italy, L/D ratio 40, D = 32 mm) equipped with a 250 mm wide sheet die and a sheet line (Trocellen QCAL-Quadro Calandra Linea R&G). The die lip was set to 1.1 mm. During

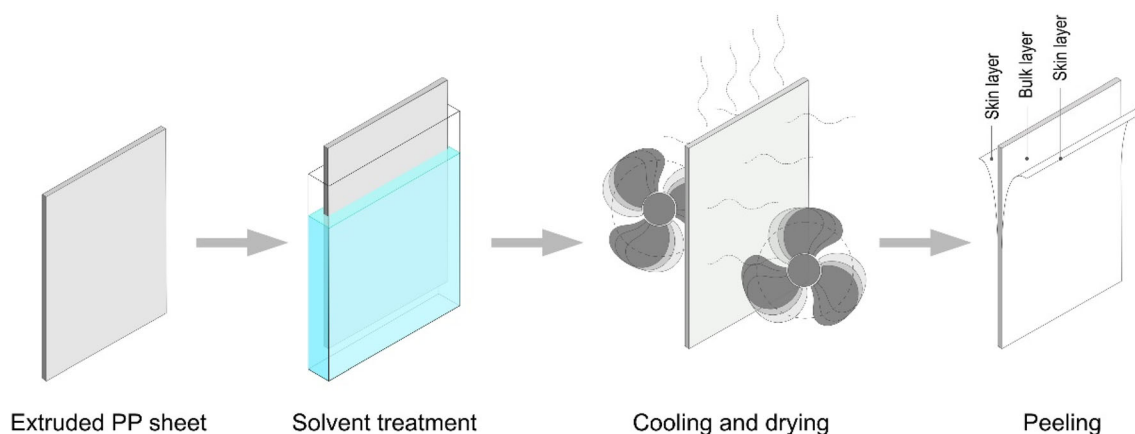Extruded PP sheet — Solvent treatment — Cooling and drying — Peeling

FIGURE 1 Schematic diagram of the solvent treatment.

extrusion, the temperature of the zones was 190, 200, 200, 200, and 200°C, the temperature of the die was 210°C, the feed rate was 5 kg/h and screw rotation speed was 60 1/min. The temperature of the conveying equipment (Trocellen QCAL-Quadro Calandra Linea R&G) was 30°C, and the pulling speed was set for the final 1 mm thickness of the sheet.

For the nucleated samples, we first produced a masterbatch with 1 wt% nucleating agent with the same co-rotating twin-screw extruder with a rod die. The applied temperature zones were 190, 200, 200, 200, and 200°C from hopper to die. The temperature of the die was 200°C and the screw speed was 20 1/min. The masterbatch was granulated with an S330 granulator (Rapid, Bredaryd, Sweden), dry-mixed, and added to the PP pellets. The final nucleating agent concentrations were 50, 500, and 1000 ppm. The sheet was extruded with settings similar to those used in the film extrusion of neat PP.

The PP samples were cut into rectangles of 150 mm × 200 mm. Figure 1 shows the schematic diagram of the solvent treatment and the subsequent steps. For the investigation of the effects of the solvent treatment parameters, the PP samples were immersed in xylene (2 L). Solvent temperatures were 120, 125, and 130°C and the duration of immersion was 30, 60, 90, and 120 s. Finally, the samples were dried at 30°C for 24 hours in an air-ventilated oven (UT6120, Thermo Fischer Scientific, USA), then for 24 hours in a vacuum oven (FCD-3000, Faithful) at 30°C.

In the drying temperature investigation, the samples were solvent-treated at 125°C for 60 s and then dried at 30, 50, 70, 80, 100, 120, and 125°C for 30 min. After drying, the samples were further dried at 30°C for 24 hours, then placed in a vacuum oven at 30°C for 24 hours in all cases. Finally, the skin layers were peeled off from both sides of the sheet.

The nucleated samples were solvent-treated at 120, 125, and 130°C for 60 and 120 s. The samples were dried at 30°C for 24 hours in an air-ventilated oven (UT6120, Thermo Fischer Scientific, USA), then for 24 hours in a vacuum oven (FCD-3000, Faithful) at 30°C.

Finally, the skin layers were peeled off as a single layer (they were not broken during peeling off) from both sides of the sheet with duct tape (Professional 4613, Tesa, Hamburg).

The remaining sheet and both sides of the peeled skin were investigated.

2.3 | Characterization of morphology

Surface and cross-section morphology were analyzed with a Jeol JSM-IT 200 scanning electron microscope (SEM). For the examination of the cross-sectional morphology, samples were cryo-fractured and made conductive by sputtering with a thin gold layer for 50 s at 10 mA in a vacuum before SEM imaging. The size of spherulites was analyzed based on the surface SEM images with the aid of the ImageJ software. For the calculation of average spherulite size, we measured the diameters of approximately 300 spherulites.

The morphology of the surface was studied with a Zeiss Axioscope polarized optical microscope (POM) equipped with a Leica DFC 320 digital camera. We analyzed crystallinity based on the images. Micrographs were recorded with the Leica IM50 software.

The nanoscale morphology of the sample surfaces was observed with a PSIA XE-100 atomic force microscope (AFM, Park Systems Corp., South Korea) in tapping mode. The data were collected in an area of 5 μm × 5 μm.

The CA was measured with the sessile drop method. To measure the advancing CA (CA$_{adv}$), we deposited a 20 μL droplet of deionized water onto the surface of the sample using a standard goniometer (Model 100–06,

Ramé-Hart Inc.). The receding CA (CA_{rec}) was measured while the volume of a sessile drop was slowly decreased by 10 μL. Each measurement was conducted at least five times across the sample surface. CA hysteresis was calculated from the difference between the advancing and receding CAs with the droplet construction and removal procedure. The shape of the drops was recorded with a high-resolution CCD camera and analyzed for CA measurements using the Image J software.

The porosity was determined from the true and apparent density according to Equation 1:

$$\varepsilon\,(\%) = \left(\frac{\rho_t - \rho_a}{\rho_t}\right) \times 100 \tag{1}$$

where ε is the porosity, and ρ_t and ρ_a are the true and apparent density of the samples, respectively.

ρ_a was determined from 4 cm × 4 cm samples. We removed the skin layer from both sides of the treated samples and measured their weight. ρ_a is obtained by dividing the weight of the samples by their volume. ρ_t was measured on an Ultra pycnometer 1000 (Quantachrome, Boynton Beach, FL, USA) with helium at 20°C.

For the specific surface area measurement, samples were cut into ca 4 mm × 4 mm pieces and degassed for 24 h at 110°C. Low-temperature (-196.15°C) nitrogen adsorption measurements were performed on a NOVA 2000 e (Quantachrome, Boynton Beach, FL, USA) automatic volumetric instrument. The apparent surface area S_{BET} was determined with the Brunauer–Emmett–Teller (BET) model.[63] From the measured apparent surface area, we determined the calculated specific surface area (S^*_{BET}), which refers to the specific surface area of the porous layer. We used the thickness of the treated samples (t_1) and the sample's bulk phase (t_2) determined from the SEM cross-section images, the apparent density (ρ_a) of the samples, and the true density (ρ_t) of the extruded sample. S^*_{BET} was calculated with the following equations:

$$V_1 = m_1 \times \rho_a \tag{2}$$

$$V_1 = t_{(3)} \times A + t_{(2)} \times A \tag{3}$$

$$t_1 = t_2 + t_3 \tag{4}$$

$$A = V_1/t_1 \tag{5}$$

$$V_2 = t_2 \times A \tag{6}$$

$$m_2 = V_2 \times \rho_t \tag{7}$$

$$m_3 = m_1 - m_2 \tag{8}$$

$$Tot_{surface} = S_{BET} \times m_1 \tag{9}$$

$$S^*_{BET} = Tot_{surface}/m_1 \tag{10}$$

where V_1, V_2, V_3 are the volume of the solvent-treated sample, the porous layer and the bulk phase, respectively. m_1, m_2, m_3 are the weight of the solvent-treated sample, porous layer and bulk phase, respectively.

The thermal analysis of the solvent-treated and annealed samples was examined by differential scanning calorimetry (DSC12E, Mettler-Toledo) in a nitrogen atmosphere. The extruded samples were immersed in silicone oil (annealing) because it does not swell PP. After that, the samples were removed and rinsed with isopropyl alcohol, and dried in air at room temperature overnight. The same temperature and the immersion time were used in silicone oil annealing and solvent-treatement. Differential scanning calorimetry was performed from 30 to 220°C at a heating rate of 10°C/min. This temperature was maintained for 5 minutes, then the samples were cooled to 30°C at a cooling rate of 10°C/min. The degree of crystallinity (X_c) was calculated with the following equation:

$$X_c = \left(\frac{\Delta H_m}{\Delta H_0}\right) \times 100 \tag{11}$$

where ΔH_m and ΔH_0 are the first melting enthalpy and melting enthalpy of a 100% crystalline sample; for PP it is 207 J/g.[64]

3 | RESULTS AND DISCUSSION

3.1 | Characterization of morphology

The surface morphology of the extruded and the unpeeled, treated sample is shown in Figure 2. The sample in Figure 2B was immersed in a 125°C solvent for 60 s.

The untreated sheet has a smooth surface (Figure 2A) due to extrusion, while after the treatment, the surface becomes rough (Figure 2B).

Figure 3 shows the surface morphology of the peeled sample and the inner side of the skin layer.

The resulting outer layer is peeled off, and the surface of the inner side of the outer layer (Figure 3B) and the peeled samples (Figures 3C,D) exhibit a sphere-like structure. The outer layer is hereinafter referred to as skin
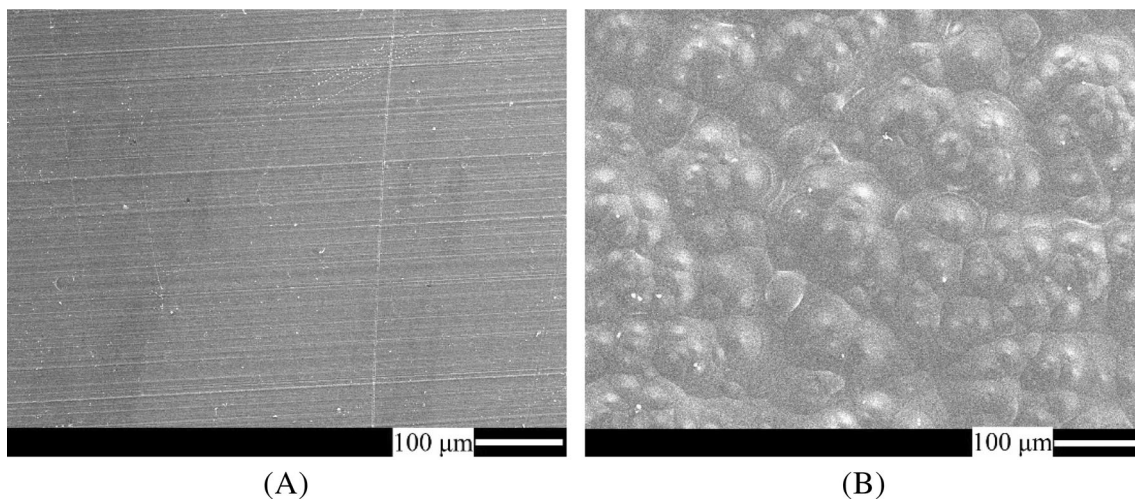
FIGURE 2 SEM images of (A) the surface of the extruded sheet and (B) the outer surface of the skin layer. The solvent temperature was 125°C and immersion time was 60 s.

FIGURE 3 POM image (A) of the inner side of the skin layer, SEM images of (B) the inner surface of the skin layer, (C) the surface of the peeled sheet, (D) is a magnification of a particle in (C). Solvent temperature was 125°C and immersion time was 60 s.
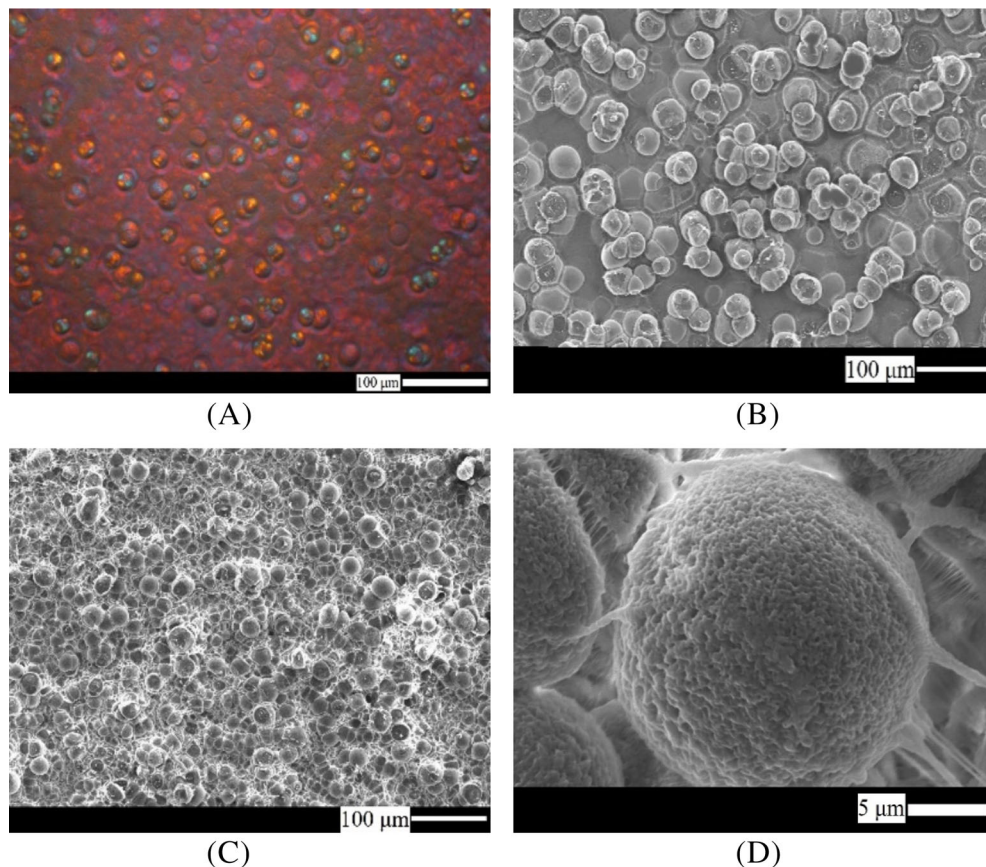
layer. Figure 3A shows the POM image of the inner side of the skin layer. The POM image reveals that the spherical structures exhibit a birefringent nature. The typical blue and yellow quarters indicative of birefringent spherulites can be seen.[65]

The surface of the peeled samples consists of regular and well-separated spherulites, which suggests that they did not interfere with each other during their growth. Similar surface topographies can be found in the literature where the surface consists of spherulites with
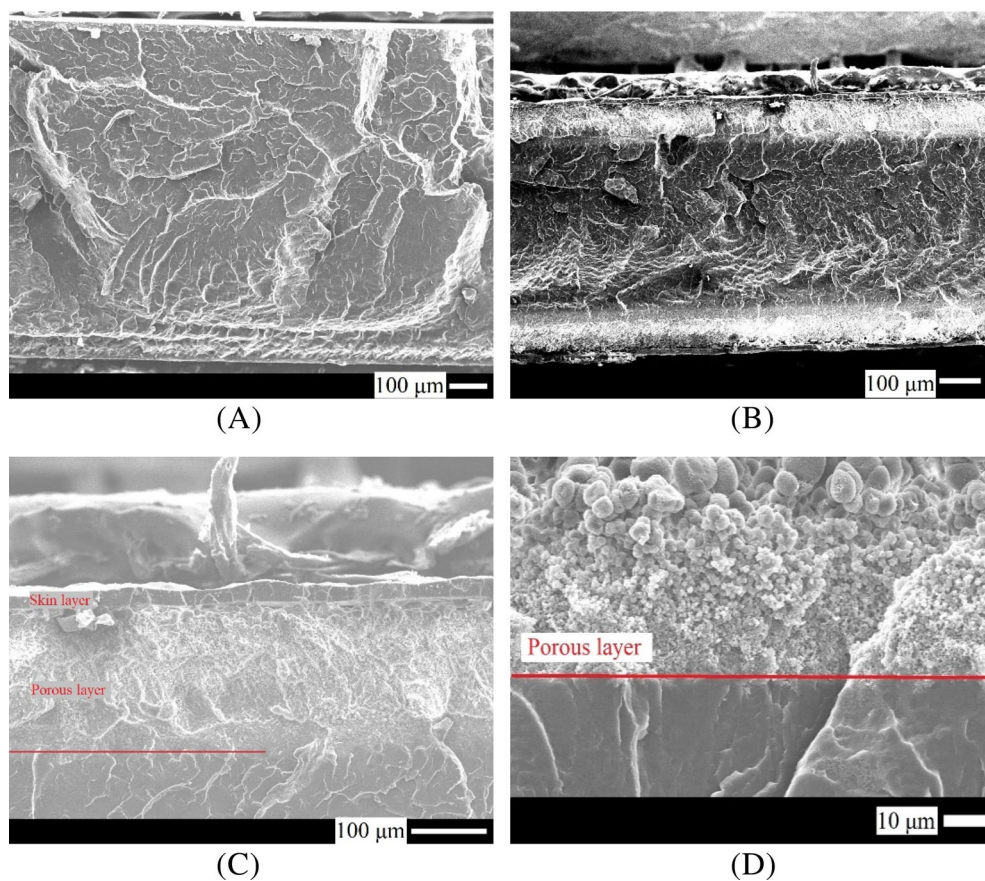
FIGURE 4 Cross-sectional SEM images of (A) the extruded PP sheet and (B) the sheet treated with a 125°C solvent for 60 s, and the treated sheet at higher magnification (C) with and (D) without the skin layer.

different sizes and voids between them, which confirm the porous nature of the surface.[66,67] The enlarged SEM image (Figure 3D) reveals that PP crystalizes as typical spherulites with a micro-and nanoscale hierarchical structure from the PP gel. The surface of spherulites also has a roughness of several tens of nanometers. The nanoscale roughness of the spherulites is a result of the radially growing branched and banded chain-folded lamellae and the solvent treatment conditions.[68]

Figure 4 shows the SEM images of the cross-section of the cryo-fractured samples after treatment. Figure 4A shows the cross-section of the extruded sheet, and Figure 4B shows the cross-section of the solvent-treated sheet before the peeling step. Figure 4C,D show the cross-section of the developed porous structure shown in Figure 4B at a higher magnification.

Under the skin layer, the cross-section has a porous layer consisting of spherulites. The size of the spherulites decreases in the direction of the bulk phase. There is a significant change in the cross-section of samples: below a certain depth, the porous structure turns into a dense material. The sharp change (marked with a red line in Figure 4C,D) shows the depth of solvent penetration into the sample. To determine the thickness of the bulk phase and the porous layer, we used this sharp boundary to distinguish the two layers. Asymmetric membranes have a structure similar to the presented porous structure and the dense layer on top of it. An important type of asymmetric membrane is an integrally skinned membrane, where the size of the pores gradually changes from very large to very fine and there is a skin layer on top of the membrane.[69]

3.2 | The effect of solvent treatment parameters on the structure

Figure 5A shows how the thickness of the skin and the porous layer of the samples changes when immersion time is varied (from 30 to 300 s) at a constant solvent temperature of 125°C. In each case, the solvent treatment step was followed by a drying step at 30°C.

The treated samples have a symmetrical structure (Figure 4B), and the porous and skin layer are formed on both sides of the samples. The presented solvent penetration depth, skin, and porous layer thicknesses in Figures 5A,B belong to one side of the treated samples.

The thickness of the skin and porous layer increases with increasing immersion time. However, after 180 s, the thickness of the layers hardly increases. Figure 5A shows that a constant thickness of the layers was achieved at 125°C.

FIGURE 5 Changes in layer thicknesses as a function of treatment time at 125°C (A) and as a function of solvent temperature with an immersion time of 60 s (B).
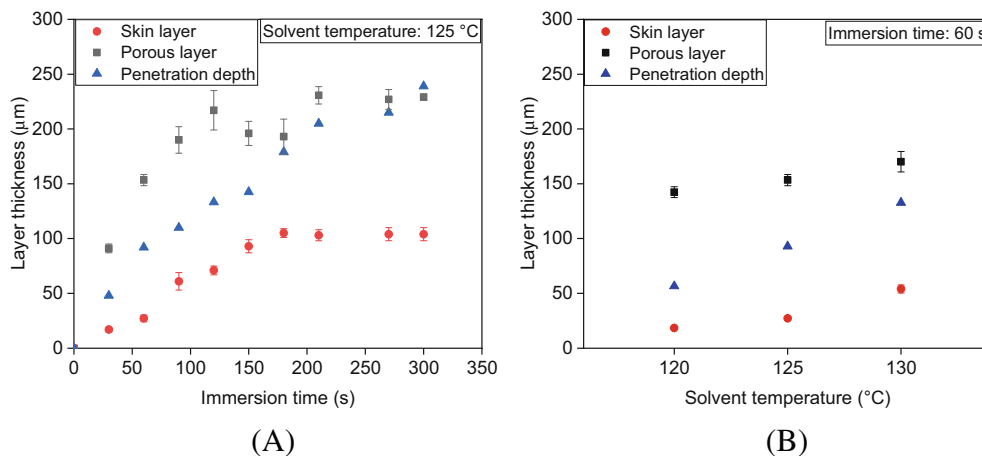

(A)

(B)

TABLE 1 Characteristics of solvent-treated PP sheets; the applied solvent temperature was 125°C.

Immersion time (s)	S_{BET} (m^2/g)	m_1 (g)	ρ_a (g/cm^3)	ρ_t (g/cm^3)	t_1 (cm)	t_2 (cm)	S_{BET}^* (m^2/g)	ε (%)
0				0.895				
30	0.8	5.16	0.79	0.905	0.108	0.904	12.6	12
60	1.9	4.50	0.73	0.912	0.112	0.816	16.3	19
90	1.6	4.94	0.68	0.911	0.116	0.780	12.5	24
150	2.7	4.07	0.69	0.911	0.110	0.715	16.3	24
210	2.5	3.91	0.62	0.914	0.105	0.590	12.4	31
280	1.5	4.58	0.56	0.911	0.980	0.570	12.7	40

Besides immersion time, solvent temperature also influences the formation of the structure. In Figure 5B, the thickness of the layers is shown as a function of solvent temperature with a constant immersion time. With increasing solvent temperature, the thickness of each layer increases.

The polymer–solvent interaction likely plays a key role in the formation of the structure created. The treatment starts with a solvent immersion step when the hot solvent diffuses into the polymer sheet through the surface and toward the center of the samples like a sharp front.[70] The solvent swells the polymer, and as a consequence, a gel layer forms in the outer region of the sheet. The degree of swelling in the gel layer decreases toward the bulk phase. The thickness of the gel layer increases over time as the solvent diffuses deeper into the polymer. In the initial period, the swelling step dominates, which increases the thickness of the gel layer. When the degree of swelling reaches a critical level, the polymer molecule becomes independent of the adjacent molecules and leaves the surface and is dissolved in the solvent. Since the loosest molecules dissolve, the thickness of the gel layer decreases. After the rate of solvent diffusion into the bulk phase and polymer dissolution reaches a steady state at the given

TABLE 2 Spherulite sizes of the solvent-treated PP sheets.

	Spherulite size (μm) Solvent temperature (°C)		
Immersion time (s)	120	125	130
30	18.7 ± 4.1	23.9 ± 4.4	30.7 ± 7.0
60	16.7 ± 3.4	23.2 ± 5.5	29.6 ± 6.2
90	20.1 ± 5.6	24.2 ± 7.1	30.8 ± 9.2
120	16.0 ± 3.9	27.5 ± 9.5	30.2 ± 7.6

solvent temperature and the gel layer with constant thickness will gradually move towards the center of the sample.[70]

During the drying step, the skin layer and the porous structure form.[71,72] First, the solvent starts evaporating from the swelled surface and this leads to the formation of the skin layer. The solidified skin layer entraps the solvent molecules underneath, so their evaporation slows down.

The formation of the spherulitic porous structure in the cross-section is a consequence of the crystallization of PP and solvent evaporation during the drying step.[71] Various studies have demonstrated that a spherulitic structure forms from a semicrystalline polymer gel.[44,73]
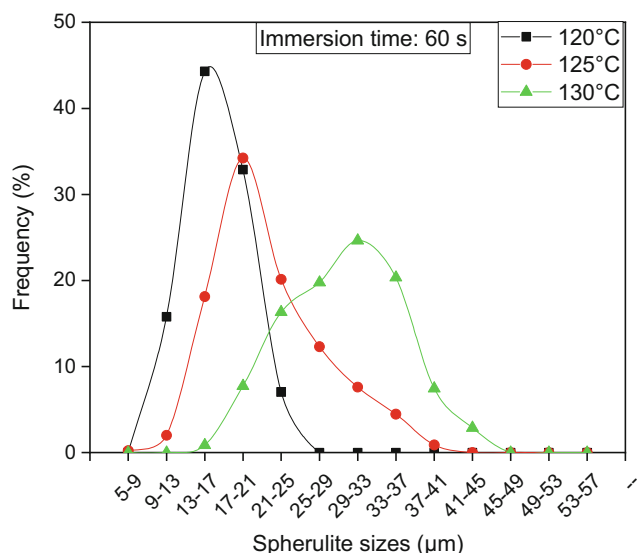
FIGURE 6 The effect of solvent temperature on the size distribution of spherulites with a constant immersion time of 60 s.

Since the evaporation of the solvent is moderate due to the skin layer, the presence of the solvent during crystallization results in the formation of separate spherical spherulites and voids among them.

Table 1 presents the measured (S_{BET}) and calculated specific surface area (S^*_{BET}) and the porosity (ε) of the samples. We took the porous layer forming on both sides of the samples into account to determine both porosity and specific surface area.

The surface-treated samples have a moderately calculated specific surface area $\left(S^*_{BET}\right)$ of about 12–16 m^2/g. As Table 1 shows, overall porosity (ε) increases with immersion time because the ratio of the porous layer and the bulk phase increases with immersion time.

The experiments with different solvent temperatures and immersion times revealed that besides the thickness of the porous and skin layers, the size of the spherulites on the porous layer also changes as solvent treatment parameters are changed. The changes in average spherulite size and its standard deviation are summarized in Table 2.

The results indicate that solvent temperature has a pronounced impact on average spherulite size. Increasing solvent temperature, results in the formation of larger spherulites from ~16 μm (120°C) to ~30 μm (130°C), regardless of immersion time, while the structure of the spherulites is constant. In comparison, spherulite sizes do not change considerably with varying immersion times at a constant solvent temperature.

The resulting porous layer consists of spherulites that form via nucleation and growth steps.[65] The crystalline structure forming during extrusion is likely disintegrated

in the swelling step and a semicrystalline gel is produced. The semicrystalline gel consists of a three-dimensional network structure, where the crosslinking points are crystallites.[44,74] These crystallites could serve as self-nuclei during crystallization. The higher the degree of swelling, the more mobile the polymer molecules are, and the more pronounced the destruction of the crystalline structure is. The molecules under the preformed skin layer have the highest mobility and kinetic energy to crystallize into quiescent spherulites. With increasing solvent temperatures and degree of swelling, fewer nuclei are present, allowing the formation of larger spherulites.[68]

Figure 6 presents the size distribution of the spherulites at different solvent temperatures with an immersion time of 60 s.

With increasing temperatures, the spherulite size distribution curves shift toward higher size ranges and broaden, which meets the expectations of spherulitic crystallization under conventional crystallization conditions from polymer melt.[75] In our case, one can speculate that at higher solvent temperatures, the original structure of the sheets formed during the extrusion disintegrates more. Consequently, during the drying step of the sheets, fewer nuclei (self-seeds, self-nuclei) are available in the treated zone to initiate the growth of spherulites, leading to bigger spherulites with a broader distribution.

The changes in crystallinity of the annealed and the solvent-treated PP sheets varying the solvent temperatures and immersion times are shown in Table 3. The reference sample is the extruded but not solvent-treated sample.

The changes in crystallinity of annealed samples were negligible compared to the reference sample, irrespective of the applied temperatures and immersion times. All the samples solvent-treated with xylene displayed an increase in crystallinity as a function of solvent temperature and immersion time. In the case of xylene-treated samples, the increased crystallinity can be attributed to the recrystallization in the solvent-affected layer and not to the recrystallization of the bulk phase.

3.3 | The effect of drying on the structure

We assumed that drying also plays a crucial role in controlling the formation of the structure, so we investigated the effect of drying temperature (between 30 and 125°C), using constant solvent treatment conditions (temperature: 125°C and immersion time: 60 s). Figure 7 shows the thickness of the skin and the porous layer at different drying temperatures.

TABLE 3 The degree of crystallinity of annealed and solvent-treated samples.

Solvent temperature (°C)	Immersion time (s)	X_c (%)	
		Silicone oil	Xylene
Reference		37.9	
120	60	38.1	39.3
125	30	37.4	37.8
	60	37.8	41.0
	90	38.5	42.2
	120	38.6	41.4
130	60	38.2	42.4
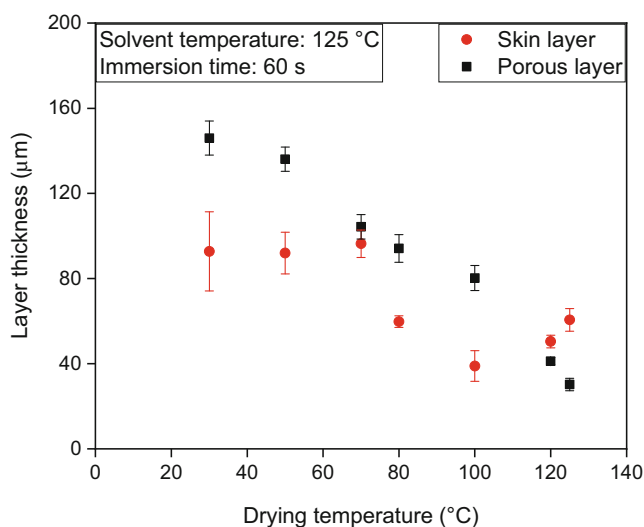
FIGURE 7 The effect of drying temperature on the structure of samples solvent-treated at 125°C for 60 s.
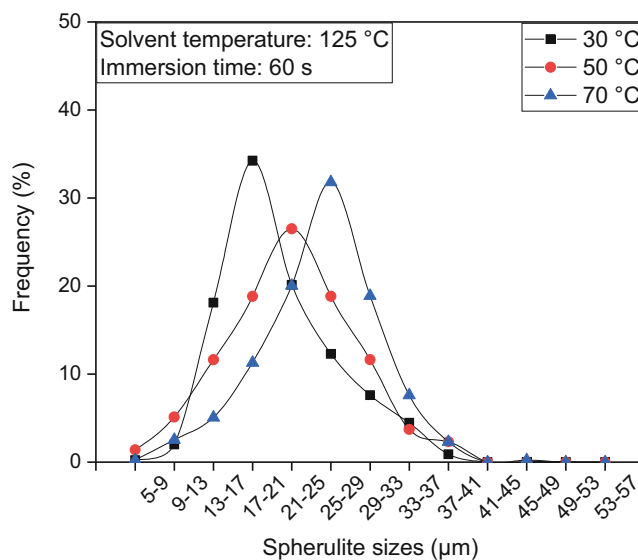

FIGURE 8 Spherulite size distribution on the samples cooled at different temperatures. The solvent treatment conditions were the same in all cases (solvent temperature is 125°C and immersion time is 60 s).

With increasing drying temperature, the thickness of the porous layer decreases; at 125°C, the porous layer almost disappears. On the other hand, there is no clear relationship between drying temperature and the thickness of the skin layer. As the porous layer becomes thinner, it is more difficult to peel off the skin layer. The drying temperature determines the time of crystal growth, the rate of solvent evaporation, and the rate at which the skin layer forms. At higher drying temperatures, the rate of solvent evaporation is higher. The observed declining trend in the thickness of the porous layer can be attributed to the higher drying temperature. At higher drying temperatures, the skin layer forms more slowly and solvent evaporation is faster, which leads to a thinner porous layer.

Figure 8 shows the relationship between drying temperature and the distribution of spherulite size on the surface of the sample after the peeling step.

The average spherulite sizes for samples dried at 30, 50, and 70°C are 23.2 ± 5.5 μm, 19.4 ± 7 μm, and

22.58 ± 5.9 μm, respectively. The calculation of the average size of spherulites is based on the size of 300 spherulites measured on the surface of the sample. The average spherulite sizes obtained at different drying temperatures are not considerably different; however, the drying temperature has an effect on the spherulite size distribution, the spherulite sizes slightly shift toward higher size ranges at higher drying temperatures. It means that the drying temperature has an effect on the temporal distribution of the nuclei formed during the crystallization. Symmetrical spherulite size distribution (Figure 8, 50°C) indicates that most of the spherulites (nuclei) formed at the same time during the crystallization. An asymmetrical size distribution shifted to the higher spherulite sizes (Figure 8, 70°C) means that more spherulites formed at the beginning of the crystallization, which was able to grow larger, while a shift to the smaller temperature

TABLE 4 Contact angles measured on solvent-treated surfaces treated at 120, 125, and 130°C for 30, 60, 90, and 120 s.

| | Solvent temperature (°C) | | | | | |
| | 120 | | 125 | | 130 | |
Immersion time (s)	CA_{adv} (°)	CAH (°)	CA_{adv} (°)	CAH (°)	CA_{adv} (°)	CAH (°)
30	155.7 ± 4.6	2.9 ± 0.2	156.2 ± 0.4	0.9 ± 0.9	157.4 ± 0.6	1.7 ± 0.5
60	156.8 ± 2.3	2.6 ± 1.7	154.9 ± 1.2	1.1 ± 0.9	156.6 ± 1.1	2.3 ± 2.1
90	151.6 ± 2.3	1.8 ± 2.9	152.9 ± 1.2	1.9 ± 1.3	155.6 ± 1.1	1.4 ± 0.7
120	154.7 ± 1.1	2.5 ± 2.9	155.6 ± 1.2	3.6 ± 0.7	154.2 ± 2.4	0.9 ± 1.1

TABLE 5 Contact angles measured on surfaces solvent-treated at 125°C for 60 s and dried at different temperatures.

Drying temperature (°C)	CA_{adv} (°)	CAH (°)
30	154.9 ± 1.2	1.1 ± 0.9
50	142.8 ± 4.2	4.7 ± 3.7
70	137.4 ± 8.5	10 ± 6.3

ranges (Figure 8, 30°C) means that the majority of the spherulites formed at close to the end of the crystallization.[75] Spherulite sizes of samples dried above 70°C are not presented because we could not peel the skin layer off the surface of these samples.

3.4 | Surface wettability of the treated samples

The untreated PP sheets showed CA_{adv} and CAH of 102° and 7°, respectively. The surface wettability results of the solvent-treated samples, dried at 30°C and peeled, are shown in Table 4.

On the treated PP samples, the increase in hydrophobicity (CA_{adv} is above 150°) and the low CAH, (less than 5°) can be attributed to the micro-, and nanoscale surface morphology, since the treatment does not affect the chemical composition of the surface, only its morphology. Due to the formation of the hierarchically structured surface morphology, the surface has superhydrophobic and water-repellent characteristics, which agrees with other published studies.[25,26]

According to the heterogeneous wetting theories, including the Wenzel and Cassie-Baxter state, the water droplet on a surface of Cassie-Baxter state shows significantly lower CAH than a surface in the Wenzel state due to the presence of liquid–air and solid–air interfaces.[76]

Our results of the CA and surface morphology analysis may indicate Cassie-Baxter's wetting mechanism of the roughened surface created.
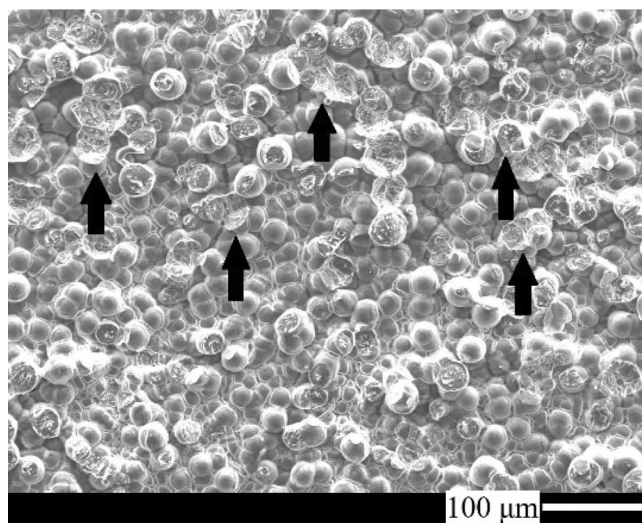
FIGURE 9 SEM images of superhydrophobic sample solvent-treated at 125°C for 60 s and dried at 70°C (the defects are shown with black arrows).

As was discussed previously, spherulite size on the surface can be tuned by solvent temperature. Therefore, we investigated the effect of spherulite size on wetting properties. Changes in spherulite sizes did not cause a significant difference in the CA due to the small change in spherulite size. Thus, changes in solvent treatment parameters do not affect the wetting behavior of the surface.

The effect of drying temperatures on surface wettability is presented in Table 5.

Drying temperature correlates more significantly with surface wettability. The higher the drying temperature, the lower CA_{adv} is and the higher CAH is. Presumably, the decreasing trend in CA_{adv} and the increasing trend in CAH are caused by the damage to the porous structure during the peeling step. As the drying temperature increased, the samples became more difficult to peel. The surface of the sample dried at 70°C is shown in Figure 9.

We were able to remove the skin layer up to 70°C, but there are many defects on the surface as the skin

FIGURE 10 SEM images of the PP surface nucleated with ADK STAB NA-21 E and treated at 125°C for 60 s. (A) containing 0 ppm (neat PP), (B) containing 50 ppm, (C) containing 500 ppm, and (D) containing 1000 ppm nucleating agent. Magnification was 1000 ×.
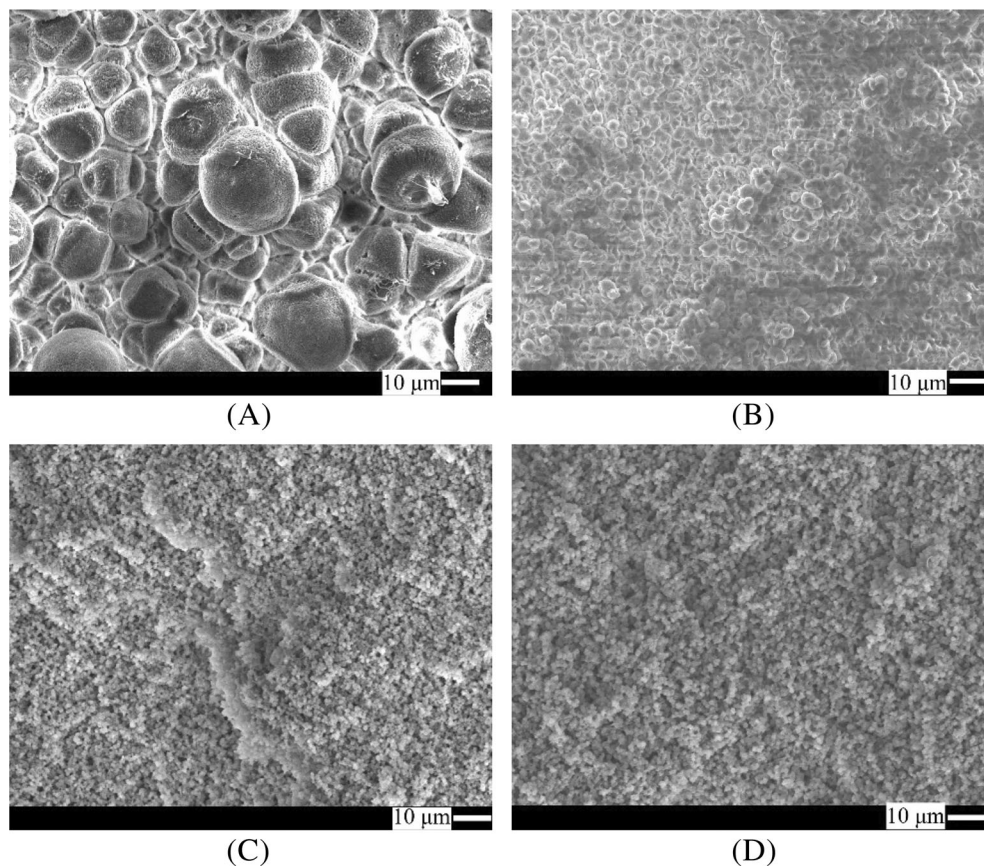

TABLE 6 Dependence of spherulite size, surface roughness, and contact angle of nucleated PP on different concentrations of nucleating agent.

Nucleating agent concentration (ppm)	Spherulite size (µm)	RMS of nanoscale roughness (nm)	CA$_{adv}$ (°)
0	23.20 ± 5.50	52	154.90 ± 1.2
50	3.37 ± 0.41	73	159.30 ± 4.2
500	1.55 ± 0.21	67	163.15 ± 1.2
1000	1.26 ± 0.15	-	163.00 ± 1.1

layer was difficult to peel. These defect points are marked with black arrows in Figure 9.

3.5 | Effect of a nucleating agent

The previously discussed results show that the surface of the extruded PP sheet can be made superhydrophobic with our method. However, by changing the parameters of the method, we cannot significantly alter surface wettability. Thus, we investigated the effect of a nucleating agent (ADK STAB NA-21 E) on micro-, and nanoscale roughness. We used a solvent temperature of 125°C and

an immersion time of 60 s. To evaluate the changes in spherulite size, we compared the surfaces of the treated neat and treated nucleated samples by SEM images (Figure 10). The nanoscale roughness of the spherulites surfaces was determined with the use of AFM topographical images. Table 6 summarizes the main surface geometry parameters and CA$_{adv}$ of the nucleated and treated samples. Nanoscale roughness is presented with its root mean square (RMS).

Spherulite size decreased from 23.2 µm ± 5.5 µm (neat PP) to 1.55 µm ± 0.21 µm for the sample with 500 ppm nucleating agent and 1.26 µm ± 0.15 for the sample with 1000 ppm nucleating agent. Figure 10 shows that spherulite sizes change slightly when the amount of NA-21 E is increased from 500 to 1000 ppm NA-21 E since the efficiency of NA-21 E reaches saturation around 500 ppm.[77] Table 6 also shows that NA-21 at and above 500 ppm reduces average spherulite size by about one order of magnitude compared to non-nucleated PP.

In the presence of a heterogeneous nucleating agent, the formation of a nucleus is more likely on the heterogeneous surface of the nucleating agent. Thus, the more crystal nuclei are created by the nucleating agent, the smaller the size of the forming spherulites is.[68]

The results indicate that the nucleating agent reduced the size of spherulites significantly, but the

TABLE 7 Spherulite sizes of the treated PP sheets nucleated with 500 ppm nucleating agent.

Immersion time (s)	Spherulite size (µm) Solvent temperature (°C)		
	120	**125**	**130**
60	1.47 ± 0.28	1.55 ± 0.21	1.50 ± 0.25
120	1.52 ± 0.31	1.50 ± 0.23	1.42 ± 0.22

nano-roughness analysis of the surfaces of the spherulites did not show remarkable differences between nucleated and non-nucleated samples (Table 6). The RMS of the nano-roughness of nucleated samples is quite similar to that of non-nucleated samples. The nano-roughness measured on the surface of the spherulites is a consequence of the chain-folded lamellae forming the spherulites and the solvent treatment conditions. Chain folding is affected by various parameters, such as crystallization temperature, chain regularity, molecular weight, and crystallization time.[78] The thickness of the chain-folded lamella depends inversely on the degree of supercooling. The similar nano-scale roughness results may be the consequence of the same treatment conditions.

Table 6 shows the effect of the nucleating agent on the CA_{adv} of the treated samples. The samples with a spherulite size below 3 µm had a CA_{adv} of more than 160°, indicating superhydrophobicity. The results suggested that increased hydrophobicity was mainly caused by the improved surface roughness as a result of the reduction in spherulite size.

Table 7 shows the effect of treatment conditions on the spherulite size of treated PP samples nucleated with 500 ppm nucleating agent.

The size of the spherulites on the surface of nucleated samples is almost identical regardless of the solvent temperature and the immersion time, contrary to the results of the previously presented neat PP samples (Table 2). In nucleated samples, the nucleus density and thus the sizes of the spherulites are mainly determined by the concentration of the nucleating agent and not by the processing conditions. Our results suggest that the number of heterogeneous nuclei can be considered almost constant after the solvent treatment, regardless of the values of the treatment parameters, so crystal growth can start from almost the same number of nuclei.

4 | CONCLUSION

We produced a hierarchically structured surface on extruded PP sheets with the combination of crystallization from a surface polymer gel layer and a skin layer

peeling step. The applied methodology is easy-to-use, and scalable, therefore, it may easily be mass-produced. The surface exhibited superhydrophobic characteristics through the formed roughened texture. The optimization of treatment parameters enables a CA higher than 155° and CA hysteresis lower than 5°. We investigated the effect of treatment parameters and the addition of a heterogeneous nucleating agent on the formation of the structure. In non-nucleated samples, the temperature of solvent treatment had a significant influence on surface texture, while the solvent treatment time affects only of the thickness of the skin and porous layer. In addition, the temperature of drying also influenced the structure. A higher drying temperature makes the skin layer more difficult to remove—above 70°C we were not able to remove it. With the addition of a nucleating agent, our method makes it possible to control surface morphology and to prepare superhydrophobic surfaces with an outstanding CA (>160°) and designable spherulite sizes.

DATA AVAILABILITY STATEMENT
The authors confirm that the data supporting the findings of this study are not available within the article.

ORCID
Csenge Vámos https://orcid.org/0000-0001-9969-9891
Tamás Bárány https://orcid.org/0000-0002-9196-7852

REFERENCES
[1] E. Celia, T. Darmanin, E. T. De Givenchy, S. Amigoni, F. Guittard, *J. Colloid Interface Sci.* **2013**, *402*, 1.
[2] N. Cherupurakal, M. S. Mozumder, A.-H. Mourad, I. Lalwani S., *Renew. Sust. Energ. Rev.* **2021**, *151*, 111538.
[3] T. He, X. Liu, Y. Wang, D. Wu, Y. Liu, X. Liu, *Appl. Surf. Sci.* **2020**, *529*, 147017.
[4] S. Xu, Q. Wang, N. Wang, *Colloids Surf. A Physicochem. Eng. Asp.* **2020**, *595*, 124719.
[5] H. Zhu, W. Hu, S. Zhao, X. Zhang, L. Pei, G. Zhao, Z. Wang, *J. Mater. Sci.* **2020**, *55*, 2215.
[6] H. Wang, X. Guo, C. Pei, W. Dong, Y. Yao, *Polym. Eng. Sci.* **2022**, *62*, 2131.

[7] L. Shen, Y. F. H. Pan, *Polym. Eng. Sci.* **2019**, *59*, E452.

[8] Y.-Y. Quan, Z. Chen, Y. Lai, Z.-S. Huang, H. Li, *Mater. Chem. Front.* **2021**, *5*, 1655.

[9] X. Zhang, J. Mo, Y. Si, Z. Guo, *Appl. Surf. Sci.* **2018**, *441*, 491.

[10] R. N. Wenzel, *Ind. Eng. Chem.* **1936**, *28*, 988.

[11] A. Cassie, S. Baxter, *Trans. Faraday Soc.* **1944**, *40*, 546.

[12] H. Wang, J. Zhuang, H. Qi, J. Yu, Z. Guo, Y. Ma, *Surf. Coat. Technol.* **2020**, *401*, 126255.

[13] H. Zheng, S. Chang, G. Ma, S. Wang, *Energ. Buildings* **2020**, *223*, 110175.

[14] H. Katouah, N. M. El-Metwaly, *React. Funct. Polym.* **2021**, *159*, 104810.

[15] F. Zhang, J. Chan, H. Y. Low, *Appl. Surf. Sci.* **2008**, *254*, 2975.

[16] N. Zhang, Y. Zhou, Y. Zhang, W. Jiang, T. F. J. Wang, *Chem. Eng. J.* **2018**, *354*, 245.

[17] A. K. Singh, J. K. Singh, *New J. Chem.* **2017**, *41*, 4618.

[18] S. N. Malakhov, S. N. Chvalun, *Polym. Eng. Sci.* **2022**, *62*, 3503.

[19] P. H. Tung, S. W. Kuo, K. U. Jeong, S. Z. Cheng, C. Huang, F. Chang F., *Macromol. Rapid Commun.* **2007**, *28*, 271.

[20] R. Menini, M. Farzaneh, *Polym. Int.* **2008**, *57*, 77.

[21] M. Zhu, W. Zuo, H. Yu, W. Yang, Y. Chen, *J. Mater. Sci.* **2006**, *41*, 3793.

[22] N. Zhao, L. Weng, X. Zhang, Q. Xie, X. X. J. Zhang, *ChemPhysChem* **2006**, *7*, 824.

[23] Y. Liao, R. Wang, A. G. Fane, *J. Membr. Sci.* **2013**, *440*, 77.

[24] J. Verma, D. Kumar, B. Sikarwar, *Polym. Polym. Compos.* **2022**, *30*, 09673911221087835.

[25] H. Y. Erbil, A. L. Demirel, Y. Avcı, O. Mert, *Science* **2003**, *299*, 1377.

[26] Y. Cao, W. Han, Z. Pu, X. Wang, B. Wang, C. Liu, H. Uyama, C. Shen, *RSC Adv.* **2020**, *10*, 26319.

[27] J.-H. Zuo, P. Cheng, X.-F. Chen, X. Yan, Y.-J. Guo, W.-Z. Lang, *Sep. Purif. Technol.* **2018**, *192*, 348.

[28] C. Fang, W. Liu, P. Zhang, S. Rajabzadeh, N. Kato, Y. Sasaki, H. Shon, K.Matsuyama H., *J. Membr. Sci.* **2021**, *618*, 118586.

[29] W. Lu, Z. Yuan, Y. Zhao, H. Zhang, H. Zhang, X. Li, *Chem. Soc. Rev.* **2017**, *46*, 2199.

[30] J. F. Kim, J. H. Kim, Y. Lee, M.Drioli E., *AICHE J.* **2016**, *62*, 461.

[31] D. R. Lloyd, K. Kinzer, E.Tseng H., *J. Membr. Sci.* **1990**, *52*, 239.

[32] J. Kim, J. Jung, H. Wang, E. Drioli, Y. M. Lee, in *Comprehensive Membrane Science and Engineering*, Second ed. (Eds: E. Drioli, Giorno L.Fontananova E.), Elsevier, United Kingdom **2017**.

[33] N. T. Hassankiadeh, Z. Cui, J. H. Kim, D. W. Shin, A. Sanguineti, V. Arcella, Y. Lee, M.Drioli E., *J. Membr. Sci.* **2014**, *471*, 237.

[34] N. Ghasem, M. Al-Marzouqi, A. Duaidar, *Int. J. Greenhouse Gas Control* **2011**, *5*, 1550.

[35] M. J. Park, C. Kim, *J. Membr. Sci.* **2014**, *449*, 127.

[36] X. L. X. Li, *J. Appl. Polym. Sci.* **2006**, *101*, 2944.

[37] Y. Jafarzadeh, R. Yegani, S. Tantekin-Ersolmaz, *Polym. Adv. Technol.* **2015**, *26*, 392.

[38] E. Afonso, A. Martínez-Gómez, P. Tiemblo, N. García, *Appl. Surf. Sci.* **2021**, *535*, 147728.

[39] Q. Zhu, Y. Yu, Q.-Y. G. L. Wu, *Chin. J. Chem. Phys.* **2017**, *30*, 219.

[40] J. Karger-Kocsis, T. Bárány, *Polypropylene handbook*, Springer Nature, Switzerland **2019**.

[41] R. Pantani, F. De Santis, V. Speranza, in *Polypropylene Handbook* (Eds: J. Karger-Kocsis, T. Bárány), Springer, Switzerland **2019**.

[42] T. Zhu, C. Cai, C. Duan, S. Zhai, S. Liang, Y. Jin, N. X. J. Zhao, *ACS Appl. Mater. Interfaces* **2015**, *7*, 13996.

[43] A. Alassod, S. R. Islam, A. X. G. Farooq, *SN Appl. Sci.* **2020**, *2*, 1.

[44] G. Andrianova, S. Pakhomov, *Polym. Eng. Sci.* **1997**, *37*, 1367.

[45] H. Matsuyama, T. Maki, M. Teramoto, K. Asano, *J. Membr. Sci.* **2002**, *204*, 323.

[46] W. Yave, R. Quijada, D. Serafini, D. R. Lloyd, *J. Membr. Sci.* **2005**, *263*, 146.

[47] K. V. Pochivalov, A. V. Basko, T. N. Lebedeva, M. Y. Yurov, A. A. Yushkin, A. V. Volkov, *J. Macromol. Sci. Part B* **2022**, *61*, 238.

[48] S. S. Kim, D. Lloyd, *J. Membr. Sci.* **1991**, *64*, 13.

[49] M. Kenneth, D. Lloyd, R.Lim G., *J. Membr. Sci.* **1993**, *79*, 27.

[50] G. B. Lim, S. S. Kim, Q. Ye, Y. Wang, F.Lloyd D., *J. Membr. Sci.* **1991**, *64*, 31.

[51] C. B. Contreras, G. Chagas, M. Strumia, D. E. C.Weibel, *Appl. Surf. Sci.* **2014**, *307*, 234.

[52] J. A. Franco, S. E. Kentish, J. Perera, M.Stevens G., *J. Membr. Sci.* **2008**, *318*, 107.

[53] S. Czyzyk, A. Dotan, H. Dodiuk, S. Kenig, *Prog. Org. Coat.* **2020**, *140*, 105501.

[54] R. Ilona, B. Marosfői, C. Vámos, Y. Nakai, Y. Mimura. Method for manufacturing machining body provided with water-repellent surface and machining body provided with water-repellent surface. 2021. JP2021013990.

[55] J.-H. Zuo, Z.-K. Li, C. Wei, X. Yan, Y. Chen, W.-Z. Lang, *J. Membr. Sci.* **2019**, *577*, 79.

[56] J. T. Jung, H. H. Wang, J. F. Kim, J. Lee, J. S. Kim, E. Drioli, Y. M. Lee, *J. Membr. Sci.* **2018**, *559*, 117.

[57] J. Zhao, L. Shi, C. Loh, H.Wang R., *Desalination* **2018**, *430*, 86.

[58] H. Karkhanechi, S. Rajabzadeh, E. Di Nicolò, H. Usuda, A. R. Shaikh, H. Matsuyama, *Polymer* **2016**, *97*, 515.

[59] S. Nejati, C. Boo, C. Osuji, O.Elimelech M., *J. Membr. Sci.* **2015**, *492*, 355.

[60] X. Zhao, W. Chen, Y. Su, W. Zhu, J. Peng, Z. Jiang, L. Kong, Y. Li, J. Liu, *J. Membr. Sci.* **2013**, *441*, 93.

[61] H. Matsuyama, M. Yuasa, Y. Kitamura, M. Teramoto, D. R. Lloyd, *J. Membr. Sci.* **2000**, *179*, 91.

[62] T. Xiao, P. Wang, X. Yang, X. L. J. Cai, *J. Membr. Sci.* **2015**, *489*, 160.

[63] S. Brunauer, P. H. Emmett, E. Teller, *J. Am. Chem. Soc.* **1938**, *60*, 309.

[64] D. Gee, T. Melia, *Die Makromolekulare Chemie* **1970**, *132*, 195.

[65] J. Molnár, Z. Zuba, Ö. Sepsi, F. Ujhelyi, G. Erdei, S. Lenk, A. Menyhárd, *Polym. Test.* **2021**, *95*, 107098.

[66] Z. Yuan, H. Chen, J. Tang, X. Chen, D. Zhao, Z. Wang, *Surf. Coat. Technol.* **2007**, *201*, 7138.

[67] N. Shirtcliffe, G. Mchale, M. Newton, C. Perry, *Langmuir* **2003**, *19*, 5626.

[68] F. Horváth, J. Molnár, A. Menyhárd, in *Polypropylene Handbook* (Eds: J. Karger-Kocsis, T. Bárány), Springer, Switzerland **2019**.

[69] B. Wang, J. Ji, K. Li, *Nat. Commun.* **2016**, *7*, 1.

[70] B. A. Miller-Chou, J. L. Koenig, *Prog. Polym. Sci.* **2003**, *28*, 1223.

[71] H. Kawakami, M. Mikawa, S. Nagaoka, *J. Membr. Sci.* **1997**, *137*, 241.

[72] K. Y. Ozawa, T. Okuzono, M. Doi, *Jpn. J. Appl. Phys.* **2006**, *45*, 8817.

[73] H. Matsuda, T. Inoue, M. Okabe, T. Ukaji, *Polym. J.* **1987**, *19*, 323.

[74] N. V. Pogodina, H. H. Winter, *Macromolecules* **1998**, *31*, 8164.

[75] J. Molnár, Ö. Sepsi, B. Gaál, Z. Zuba, M. Dobrzyńska-Mizera, A. Menyárd, *Mater. Des.* **2021**, *212*, 110245.

[76] G. Heydari, E. Thormann, M. JäRn, E. Tyrode, P. M. Claesson, *J. Phys. Chem. C* **2013**, *117*, 21752.

[77] A. Menyhárd, M. Bredács, G. Simon, Z. Horváth, *Macromolecules* **2015**, *48*, 2561.

[78] B. Wunderlich, *Crystal Structure, Morphology*, Academic Press, Defects. Macromolecular Physics. London **1973**.